BMC Gastroenterology

RESEARCH

Open Access

Single-cell transcriptomic landscape of intrahepatic B Cells in MASH

Jia-Chun Lu[1†], Min-Li Xiong[5†], Zhi-Qi Cai[2,3†], Ting Mao[1†], Long Tang[2,3], Hui-Yi Li[1], Ming-Yi Xu[1*] and Sheng-Zheng Luo[2,3,4*]

Abstract

To understand the heterogeneity of single-B cell responses to Metabolic Dysfunction-Associated Steatohepatitis (MASH), we performed Single-cell RNA sequencing (scRNA-seq) on single-B cells isolated from control and MCD-fed mice livers. Subsequent analyses included clustering, identification of differentially expressed genes (DEGs) and enrichment analysis. The expressions of high specific DEGs were validated using quantitative real-time PCR (qRT-PCR), immunofluorescence staining and function study. Four single-B cell clusters (3, 14, 16 and 20) were identified. The total number and proportion of B cells significantly decreased in MASH mice livers. In cluster 3, the decreasing *Fcer2a*$^+$ mature B cells were supposed with anti-inflammatory role associated with B cell activation and differentiation of other immune cells in MASH. The DEGs (*Fcer2a*, *Cd22*, *Cr2* and *Fcmr*) of cluster 3 were consistently downregulated in B cells cocultued with lipotoxic hepatocytes. And the portal area of livers contained fewer *Fcer2a*$^+$ B cells in MASH patients and mice compared with controls. *Fcer2a*$^+$ B cells attenuated lipotoxicity-driven inflammation by enhancing anti-inflammatory factor (IL-10, IL-35) secretion and inhibiting T cell inflammatory factor (IFN-γ, TNF-α, IL-17) production and proliferation. The other 3 clusters (14, 16 and 20) contained small numbers of single-B cell. *Tnfrsf17*$^+$ plasmacytes (PCs) of cluster 14 were identified with the effect related to endoplasmic reticulum stress and N-Glycan biosynthesis. *Klk1*$^+$ B cells of cluster 16 were implicated in regulating immune response in MASH. *Apol7c*$^+$ B cells of cluster 20 participated in apoptosis, NF-κB, TNF and JAK-STAT signaling pathway in MASH. Thus, a subgroup of *Fcer2a*$^+$ mature B cells, diminished in MASH, may exerted anti-inflammatory or immunosuppressive effects.

Keywords Metabolic Dysfunction-Associated Steatohepatitis, B cell; single-cell RNA sequencing, Fcer2α

†Jia-Chun Lu, Min-Li Xiong, Zhi-Qi Cai and Ting Mao contributed equally to this work.

*Correspondence:
Ming-Yi Xu
xumingyi@tongji.edu.cn
Sheng-Zheng Luo
luoshengzheng2007@163.com

[1]Department of Gastroenterology, Shanghai East Hospital, School of Medicine, Tongji University, Shanghai 200123, China
[2]Ningde Municipal Hospital, Ningde, Fujian 355099, China
[3]Ningde Clinical Medical College of Fujian Medical University, Ningde, Fujian 352101, China
[4]Department of Gastroenterology, Shanghai General Hospital, Shanghai Jiaotong University, School of Medicine, Shanghai 200080, China
[5]Outpatient Department of Shanghai University of International Business and Economics, Shanghai 201620, China

Introduction

Metabolic dysfunction-associated steatotic liver disease (MASLD) affects approximately 38% of the global population and represents the most prevalent chronic liver disease worldwide [1]. Up to 20% of MASLD cases progress to non-alcoholic steatohepatitis (MASH), which is characterized by sustained hepatocellular injury, chronic inflammation, and fibrogenesis, ultimately predisposing patients to cirrhosis, hepatocellular carcinoma, and liver-related mortality [2].

Emerging evidence implicates hepatic B cells in the pathogenesis of MASH, particularly through modulation of the B cell–activating factor axis and promotion of oxidative stress [3]. Nevertheless, the precise mechanisms by which B cells contribute to MASH remain incompletely understood. Single-cell RNA sequencing (scRNA-seq), a powerful tool enabling transcriptomic profiling at single-cell resolution, has recently been leveraged to unravel novel immune cell heterogeneity and functional states in MASH [4, 5]. For instance, Barrow et al. identified three distinct hepatic B cell clusters, including mature B cells, immature B cells, and metabolically active subsets enriched in mitochondrial genes [4]. In parallel, Kotsiliti et al. reported increased intestinally derived activated B cells in both murine and human MASH, accompanied by elevated IgA levels and enhanced FcRg$^+$ myeloid cell activity, which correlated positively with fibrosis severity [5]. These findings underscore the multifaceted roles of B cells in shaping the immunopathological landscape of MASH.

Here, we performed scRNA-seq of liver nonparenchymal cells (NPCs) from MASH and control mice to systematically dissect intrahepatic B cell heterogeneity. We identified four transcriptionally distinct B cell subsets and observed marked compositional changes in MASH. Notably, Fcer2α$^+$ B cells were significantly reduced, suggesting a loss of their potential anti-inflammatory capacity. In addition, we characterized Tnfrsf17 + plasmacytes, Klk1$^+$ B cells, and Apol7c$^+$ B cells, each exhibiting unique transcriptional signatures and functional enrichment patterns, whose potential roles in MASH remain to be experimentally validated. Collectively, these findings provide new insights into B cell biology in fatty liver disease and establish a framework for exploring their functional relevance as potential immunotherapeutic targets.

Methods and materials

Human samples

A total of six MASLD patients were enrolled. All patients underwent biopsy confirming MASLD diagnosis based on pathological steatosis scores. Patients were divided into two groups: mild MASLD and advanced MASH ($n = 3$ per group). Cohort details are provided in Table S1. Written informed consent was obtained from all participants, and the study was approved by the ethics committee of Shanghai East Hospital.

MASH mouse model

Twelve C57BL/6N mice (8 weeks of age, male) were fed with a standard diet (control group) or a methionine-choline deficient diet (MCD, MASH group) for 6 weeks ($n = 6$ per group).The experimental animals were purchased from Shanghai Slek Laboratory Animal Co., Ltd. and the mice were sacrificed by cervical dislocation. Three pairs were used for scRNA-seq and three pairs for immunofluorescence staining.

Histological identification of MASH patients and mice

Human liver tissue sections were prepared and stained with hematoxylin–eosin (H&E). Mouse liver tissue sections were stained with H&E, Masson's trichrome (Masson) and Oil Red O (ORO). Immunohistochemistry (IHC) for liver macrophages was performed using an anti-mouse F4/80 antibody, and F4/80-positive cells were counted. Steatohepatitis, lipid droplets, fibrosis and inflammatory infiltration of liver were assessed by light microscopy (Leica Microsystems, Wetzlar, Germany). Images were analyzed using Image J 1.8.0 software (National Institutes of Health, USA). MASH activity scores were evaluated by a pathologist based on established criteria [6], considering steatosis, inflammation, and ballooning degeneration.

scRNA-seq and data analysis

Liver tissues from MASH and control mice ($n = 3$ per group) were subjected to scRNA-seq (Sinotech Genomics Co. Ltd., Shanghai, China) as our previous research [7]. Details on single-cell suspension preparation, transcriptome processing, library construction, and sequencing are provided in the supplemental file. Single cell data dimensionality reduction was performed using t-distributed stochastic neighborhood embedding (t-SNE). Feature plots, violin plots and heatmap were used to visualize the expression of the differentially expressed genes (DEGs). Specific marker genes for each cluster were identified using the FindAllMarkers function (Wilcoxon test; criteria: $|\log2\text{-fold change}| > 0.25$, min. percentage > 0.25) in Seurat 4.0. Cell type annotation for the cell subpopulations was performed using the built-in mouse RNA-sequencing reference dataset within the R package Single R 1.4.1. B cells were identified based on the expression of cluster of differentiation 79a (*Cd79a*), cluster of differentiation 19 (*Cd19*) and membrane spanning 4-domains α l (*Ms4α1*). The average of logFC (avg-logFC) and the percentage of FC (pct_FC) represented the enrichment of the DEGs in corresponding cluster. To explore the related function and signal pathways of DEGs, gene ontology (GO) and Kyoto Encyclopedia of Genes and Genomes

(KEGG) were analyzed by Cluster Profiler package. GO analysis contained biological process (BP), cellular component (CC) and molecular function (MF).

Cell line and culture

For cell culture, HepG2 cells, GM12878 cells and Jurkat cell lines were obtained from the Shanghai Cell Bank in the Chinese Academy of Sciences. HepG2 cells (human hepatocellular carcinoma cell line) were cultured in Dulbecco's Modified Eagle Medium (DMEM, Gibco, CA, USA) with 10% Fetal Bovine Serum (FBS, Gibco) and 1% penicillin–streptomycin (Invitrogen, Carlsbad, CA). GM12878 cells (human B lymphocyte line) were cultured in complete Roswell Park Memorial Institute-1640 (RPMI-1640, Gibco) containing 15% FBS and 1% penicillin–streptomycin. Jurkat cells (human T lymphocyte line) were cultured in RPMI-1640 with 10% FBS (Gibco). All cells were grown at 37 °C with 5% CO_2.

B cell line (GM12878 cells) transfection

The pCMV-MCS-3flag vector (HANBIO, Shanghai, China) and the full-length fragments of *Fcer2α* were double digested and ligated with T4 DNA ligase (Takara, Kyoto, Japan). After construction, the plasmids were verified by sequencing. GM12878 cells (1×10^5 cells/well) in 6-well plates were transfected with *Fcer2α* overexpression plasmid (ov-*Fcer2α*) or negative control plasmid (ov-NC) using Lipofectamine 3000 (Invitrogen, Carlsbad, US) for 48 h in accordance with the manufacturer's instructions.

B cells-hepatocytes coculture

To assess the effects of hepatocyte-derived factors on B cells in lipotoxic environment, HepG2 cells were incubated for 24 h with serum-free DMEM containing either bovine serum albumin (BSA, BioFroxx; CM-BSA group) or palmitic acid (PA, 200 μmol/L, Sigma; CM-PA group). The conditioned medium (CM) was collected and filtered (0.22 μm). GM12878 cells (2×10^5 cells/well in 6-well plates) were cultured for 24 h with a 1:1 mixture of CM (CM-BSA or CM-PA) and RPMI-1640 complete medium.This conditioned-medium design was conceptually informed by prior HepG2-based immune-interaction models used in MASLD/MASH research to interrogate hepatocyte-to-immune inflammatory signaling [8].

To verify the function of *Fcer2α*$^+$ B cells in a lipotoxic environment, ov-*Fcer2α* or ov-NC GM12878 cells were established. After 24 h, transfected cells were treated with CM-PA (1:1 with RPMI-1640) for an additional 24 h. Then, GM12878 cells were harvested for RNA extraction.

B cells-T cells coculture

B cell-T cell interactions were assessed using a Transwell coculture system (0.4 μm pore polyester membrane, Corning Inc., Corning, NY, USA). GM12878 cells (2.5×10^5) transfected with either ov-*Fcer2α* or ov-NC plasmids and pre-conditioned with CM-PA were seeded in the upper chamber of 24-well plates. Jurkat cells (5×10^5) were placed in the lower chamber. After 24 h coculture at 37 °C/5% CO_2, Jurkat cells were harvested for parallel analyses: (1) Total RNA was extracted for qPCR quantification of pro-inflammatory cytokine. (2) EdU$^+$ cell proliferation assessment. All conditions were run in technical triplicates with three independent biological replicates.

EdU cell proliferation assay

Cellular proliferation was quantified using the Click-iT EdU-594 kit (Servicebio, Wuhan, China) according to the manufacturer's protocol. Briefly, cells were pulsed with 10 μM EdU for 2 h prior to fixation. After washing with PBS, cells were fixed with 4% paraformaldehyde (15 min), permeabilized with 0.5% Triton X-100 (20 min), and incubated with click reaction solution containing fluorescent dye iF594 for 30 min protected from light. Nuclei were counterstained with Hoechst 33,342 staining solution (1 μg/mL, 10 min). Images were acquired on a TCS SP8 CARS fluorescence microscope (Leica Microsystems) and analyzed using ImageJ (v1.8.0) to calculate the EdU$^+$/Hoechst$^+$ ratio.For flow cytometric detection of EdU, after EdU labeling, cells were harvested and centrifuged at 1000 rpm for 5 min, fixed with 4% paraformaldehyde for 15 min at room temperature, washed three times, permeabilized with PBS containing 0.3% Triton X-100 for 15 min, and washed twice. The Click reaction solution (iF594) was freshly prepared according to the manufacturer's instructions and used within 15 min; cells were incubated with 0.5 mL reaction solution for 30 min at room temperature in the dark. After three washes, EdU-positive cells were quantified by flow cytometry on the FL3 (PerCP) channel, and data were analyzed using FlowJo (v10.8.1).

Quantitative real-time PCR (qRT-PCR)

QRT-PCR used the SYBR Green PCR Kit (Yeasen Biotech Co. Ltd., Shanghai, China). The primers were showed (Sangon Biotech Co., Ltd., Shanghai, China, Table S2).

Immunofluorescence (IF) assay

IF staining of liver tissues was examined employing of anti-Cd79a (as B cell marker), anti-Fcer2α and anti-Tnfrsf17 at a 1:200 dilution (Table S3). Nucleus were stained with DAPI. Images were captured (TCS SP8 CARS fluorescence microscope, Leica Microsystems), and relative percentage of positive cell area was calculated.

Flow cytometric analysis of hepatic B Cell Subsets

Liver tissues were mechanically minced into approximately 1 mm pieces and washed with PBS. The tissue fragments were digested with collagenase (50–200 U/mL) in RPMI 1640 (Gibco) at 37 °C for 10 min with intermittent agitation. Digestion was terminated with 3% FBS (Gibco), and the suspension was filtered through a 70-μm cell strainer (Biosharp, Beijing, China) to remove debris. After centrifugation (1000 rpm, 5 min), cells were resuspended in PBS to a density of 1×10^7 cells/mL. The cell suspension (125 μL/well) was seeded in 96-well plates, supplemented with complete RPMI-1640, and stimulated with PMA and BFA for 4–6 h at 37 °C. Following incubation, cells were stained with fluorochrome-conjugated antibodies, including FITC Anti-Mouse CD45 (Proteintech, Wuhan, China), APC Anti-Mouse CD19 (Elabscience, Wuhan, China), and PE Anti-Mouse CD23 (Elabscience) for 30 min at 4 °C in the dark. Unstained and single-stained controls were established for compensation. Cells were then washed and subjected to fixation and permeabilization followed by data acquisition using a flow cytometer.

Statistical analysis

For scRNA-seq, wilcoxon test and Bonferroni correction built in Seurat package (version 4.0) of R software were used to analyze DEGs; fisher exact test and false discovery rate correction were performed on GO and KEGG data using ClusterProfiler package. In qRT-PCR and IF experiments, differences between 2 groups were analyzed with unpaired Student's t test (p-value < 0.05 was statistically different).

Results

Identification of single-B cell clusters in livers of MASH mice

The MASH activity score, degree of liver fibrosis and lipid deposition, as well as the percentage of F4/80-positive area, were markedly higher in the livers of MCD-fed mice compared with controls (Fig. S1), confirming the successful establishment of the MASH model. The MCD model was selected because previous studies confirmed that the MCD diet can reproduce liver lymphocyte responses associated with human MASLD/MASH [9, 10]. Our study focused on investigating the intrahepatic immune microenvironment, particularly the phenotypic and functional alterations of liver-resident B cell subsets during steatohepatitis. The MCD model remains a useful tool for probing local immune mechanisms that contribute to disease progression. However, it is important to note that the MCD model does not fully recapitulate the metabolic dysregulation characteristic of human MASLD/MASH.

Nonparenchymal cells (NPCs) isolated from liver tissues of MASH and control mice were subjected to scRNA-seq, as described previously [7]. B cells were identified based on the expression of canonical markers Cd79a, Cd19, and Ms4a1 (CD20) (Fig. 1C). A total of 1,106 and 581 B cells were obtained from control and MASH livers, respectively, revealing a significant reduction in both the absolute number and proportion of B cells in MASH.

To further characterize B cell alterations, t-SNE analysis was applied to cluster single B cells. Four subsets (clusters 3, 14, 16, and 20) were identified, each displaying distinct abundance patterns between control and MASH groups (Fig. 1A). The proportions of clusters 3 and 14 within NPCs were decreased in MASH, whereas cluster 20 was increased (cluster 3: 10.45% vs. 14.64%; cluster 14: 3.72% vs. 5.80%; cluster 20: 2.12% vs. 1.44%; MASH vs. control, Fig. 1B). Notably, the distribution of clusters 3, 14, and 16 within the total B cell population remained largely unchanged, except for cluster 20, which was enriched in MASH (Fig. 1B). An unsupervised heatmap highlighted the top 10 differentially expressed genes (DEGs) for each subset, based on relative expression intensity (Fig. 1D).

The characteristics of a cluster of Fcer2α + B cells

The proportion of cluster 3 B cells was markedly reduced in MASH. Notably, cluster 3 represented the predominant B cell population among the four subsets (Fig. 1B). This cluster annotation was primarily supported by the literature-based interpretation of the four top marker genes (Fcer2α, Cr2, Fcmr, and Cd22), and was characterized by enriched expression of these markers together with six additional differentially expressed genes (Cxcr5, Bank1, B3gnt5, Serpinb1a, Zfp318, and Ighd), as visualized by t-SNE and violin plots (Fig. 2A–D; Table S4). Fcer2α (also known as Cd23), a low-affinity IgE receptor, is highly expressed on mature B cells, particularly the B2 subset [11]. Cr2 (Cd21) expression is dynamically regulated during B lymphopoiesis and coincides with B cell maturation [12]. Fcmr (also termed TOSO/FAIM3), selectively expressed by lymphocytes, modulates B cell receptor (BCR) signaling through interactions with spleen tyrosine kinase [13]. Cd22 (Siglec-2), another classical B cell marker, is also frequently used in identifying malignant B cells [14]. Approximately 60% of cluster 3 B cells expressed Fcer2α, supporting its designation as the most specific marker gene for this cluster (Table S4), thereby identifying it as a *Fcer2α*$^+$ B cell subset.

Gene Ontology (GO) enrichment analysis revealed biological processes (BP) associated with B cell activation, B cell differentiation, lymphocyte differentiation, lymphocyte proliferation, and T cell activation; cellular components (CC) enriched for major histocompatibility complex (MHC) protein complex, membrane raft, and immunological synapse; and molecular functions (MF) including MHC protein complex binding, transcriptional

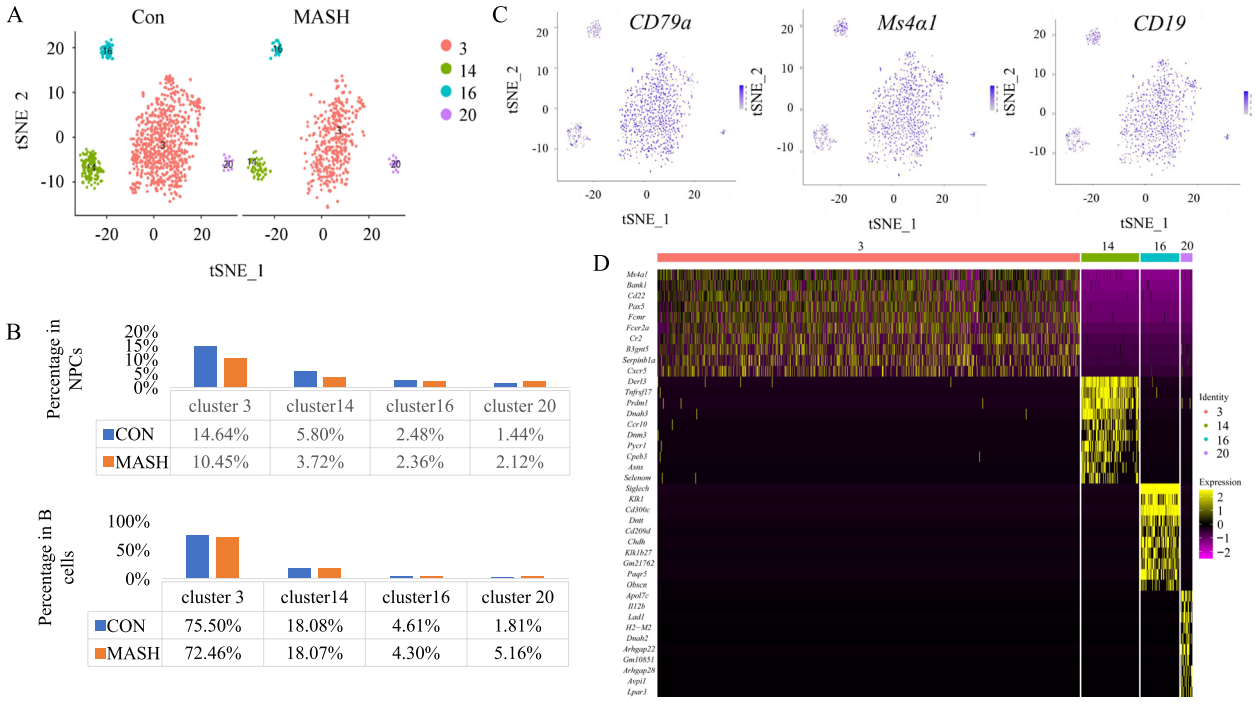

Fig. 1 Four B cell subsets isolated from mouse livers. **A** t-SNE plots of B cells in liver tissue from control and MASH mice by scRNA-seq (each group, $n = 3$). **B** Comparison of B cell percentage of NPCs or total B cells in each cluster between the control and MASH groups. **C** The t-SNE plots showed the expression levels of the B cell markers of *Cd79a*, *Cd 19* and *Ms4a1*.**D** Heatmap of the top 10 specific DEGs in 4 B cell clusters (3, 14, 16 and 20)

co-regulator activity, transcriptional co-activator activity, and NF-kappaB binding (Fig. 2E). KEGG pathway analysis further demonstrated significant enrichment in Th1/Th2/Th17 cell differentiation, BCR signaling pathways, and NF-kappaB signaling pathway. (Fig. 2E).

Together, these findings indicate that MASH is associated with a depletion of *Fcer2a*$^{+}$ B cells.Functional enrichment analyses suggest that this subset is transcriptionally linked to B-cell activation/differentiation and pathways related to T-cell differentiation and immune signaling, supporting a potential role in modulating the inflammatory microenvironment in MASH.

The characteristics of a cluster of Tnfrsf17 + plasmacytes (PCs)

The proportion of cluster 14 B cells was also reduced in MASH (Fig. 1B). Cluster 14 distinctly expressed *Asns*, *Pycr1*, *Dnm3*, *Ccr10* and other 6 DEGs [TNF receptor superfamily 17(*Tnfrsf17*), dynein axonemal heavy chain 3(*Dnah3*), *Cpeb3*, PR domain-containing protein 1(*Prdm1*), *Derlin-3*(Derl3) and *Selenom*], as revealed by t-SNE and violin plot analyses (Fig. 3A–D; Table S5). Among these, four DEGs (Tnfrsf17, Dnah3, Prdm1, and Derl3) were expressed in more than 50% of B cells in this cluster (Table S5). *Tnfrsf*17, encoding for B cell maturation antigen, is a receptor involved in B cell activating factor affecting on cells [15] and predominates on plasmablasts and PCs [16]. *Prdm1-IRF4* signaling activation would encode *Blimp1* in B lineage cells and initiate PCs differentiation [17]. *Derl3* was enriched in PCs of the B cells [18]. *Dnah3* is a spermatogenesis related gene; its role in B cells is still unclear. Nearly 72% of cluster 14 cells expressed Tnfrsf17, ranking fifth in pct-FC values (Table S5), thereby establishing Tnfrsf17 as the defining marker gene of this cluster and identifying it as a plasma cell subset.

GO enrichment analysis highlighted BP related to endoplasmic reticulum (ER) stress responses, including unfolded and misfolded protein processing; CC enriched in the ER chaperone complex, ER lumen, smooth and rough ER; and MF associated with misfolded/unfolded protein binding, mannosidase activity, and ubiquitin-specific protease binding (Fig. 3E). KEGG pathway analysis revealed significant enrichment in ER protein processing and N-glycan biosynthesis pathways (Fig. 3E).

Collectively, these findings identify an intrahepatic Tnfrsf17^{+} plasma cell subset that is reduced in MASH. Transcriptomic enrichment suggests an association with ER stress responses and N-glycan biosynthesis; however, the functional contribution of this subset to MASH pathogenesis requires further protein-level or functional validation.

The characteristics of a cluster of Klk1 + B cells

The proportion of cluster 16 B cells was comparable between MASH and control groups (Fig. 1B). Cluster

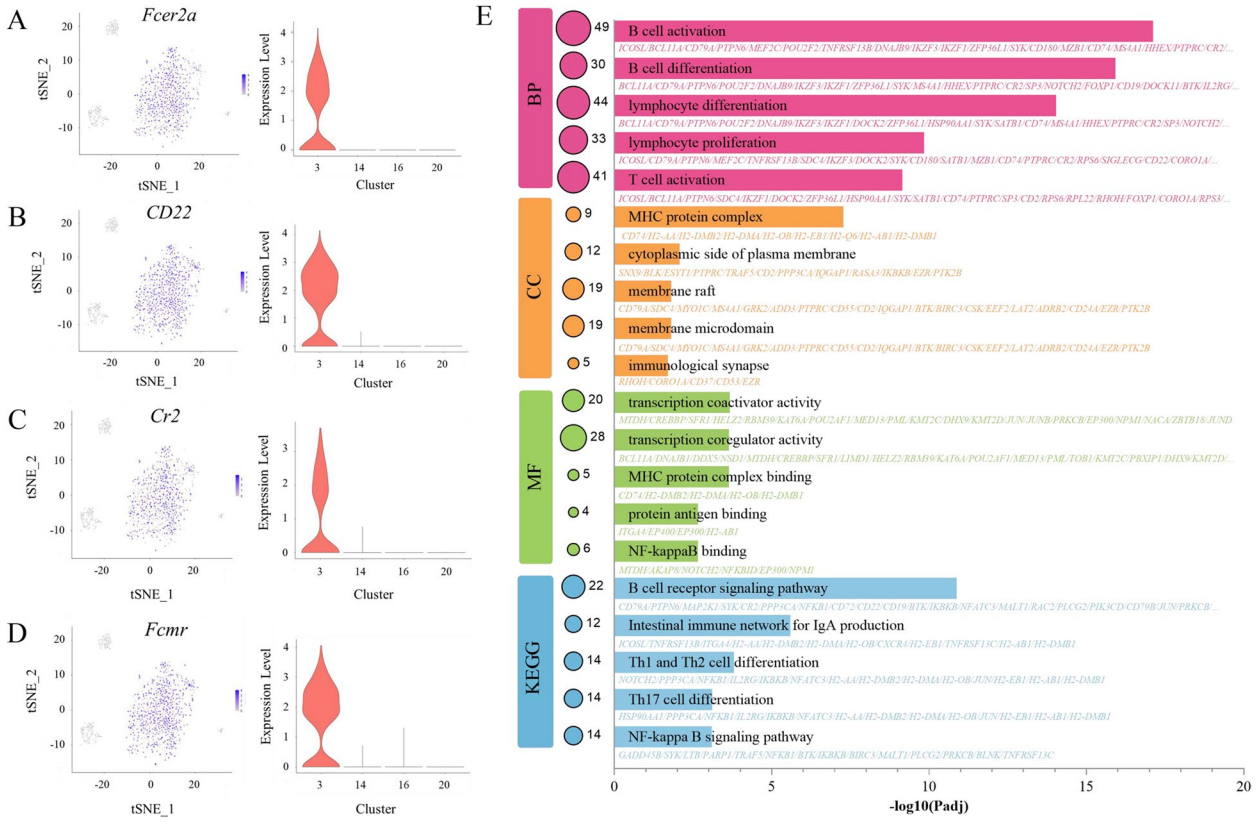

Fig. 2 Characteristics and biological functions of B cells in cluster 3. **A**-**D** Paired t-SNE plots (left) and violin plots (right) showed the expression levels of specific DEGs including *Fcer2a* (**A**), *Cd22* (**B**), *Cr2* (**C**) and *Fcmr* (**D**) in cluster 3. (**E**) GO analysis and KEGG pathway enrichment of B cells distributed in cluster 3

16 specifically expressed *Klk1* (kallikrein related peptidase 1), *Chdh* (choline dehydrogenase), *Dntt* (terminal deoxynucleotidyl transferase), *Paqr5* and other six DEGs (*Gm21762*, *Klk1b27*, *Cd209d*, *Obscn*, *Atp2a1* and *Smim5*),as revealed by t-SNE and violin plot analyses (Fig. 4A–C; Table S6). Among them, three genes—Klk1, Chdh, and Dntt—were expressed in more than 55% of B cells within this cluster (Table S6). *Klk1* (tissue kallikrein), a widespread serine protease, typically inhibits kallistatin activity [19]. Nearly 71% of cells in cluster 16 expressed Klk1, with the highest pct-FC value among all DEGs (Table S6), thereby establishing Klk1 as the defining marker gene of this cluster.

GO enrichment analysis indicated BP related to T cell activation, T cell differentiation, and regulation of T cell activation; CC associated with lysosome, lytic vacuole, MHC protein complex, phagocytic vesicle, and endocytic vesicle; and MF including transcription coregulator/corepressor activity, cytokine receptor activity, unfolded protein binding, and MHC protein binding (Fig. 4D). KEGG pathway analysis further revealed significant enrichment in protein processing in ER, antigen processing and presentation, BCR signaling, Lysosome and Phagosome (Fig. 4D).

Taken together, these data identify a hepatic Klk1⁺ B cell subset in MASH.Its putative involvement in antigen presentation, BCR signaling, and T-cell–related pathways is inferred from GO/KEGG enrichment and should be interpreted cautiously until supported by direct functional validation.

The characteristics of a cluster of very few Apol7c + B cells

The proportion of cluster 20 B cells, which represented the smallest subset, was further reduced in MASH (Fig. 1B).Cluster 20 specifically expressed of *Apol7c* (apolipoproteins L7c), *Lad1* (leukocyte adhesion deficiency 1), *Arhgap22* (Rho GTPase activating protein 22), *Arhgap28* and other 6 DEGs (*Gm10851*, *Il12b*, *H2-M2*, *Dnah2*, *Avpi1* and *Lpar3*),as revealed by t-SNE and violin plot analyses (Fig. 5A–C; Table S7). Three major DEGs (*Apol7c*, *Lad1*, *Arhgap22*) were enriched in > 50% B cells of this cluster (Table S7). *Apol7c* (in mouse, or *Apol1* in human) was found to bind Bcl-xL (anti-apoptosis) to mediate cell death [20]. The functions of these DEGs were unclear in B cells and MASH. Notably, 57% of cluster 20 cells expressed Apol7c, which also exhibited the highest pct-FC (Table S7), establishing Apol7c as the defining marker gene of this cluster.

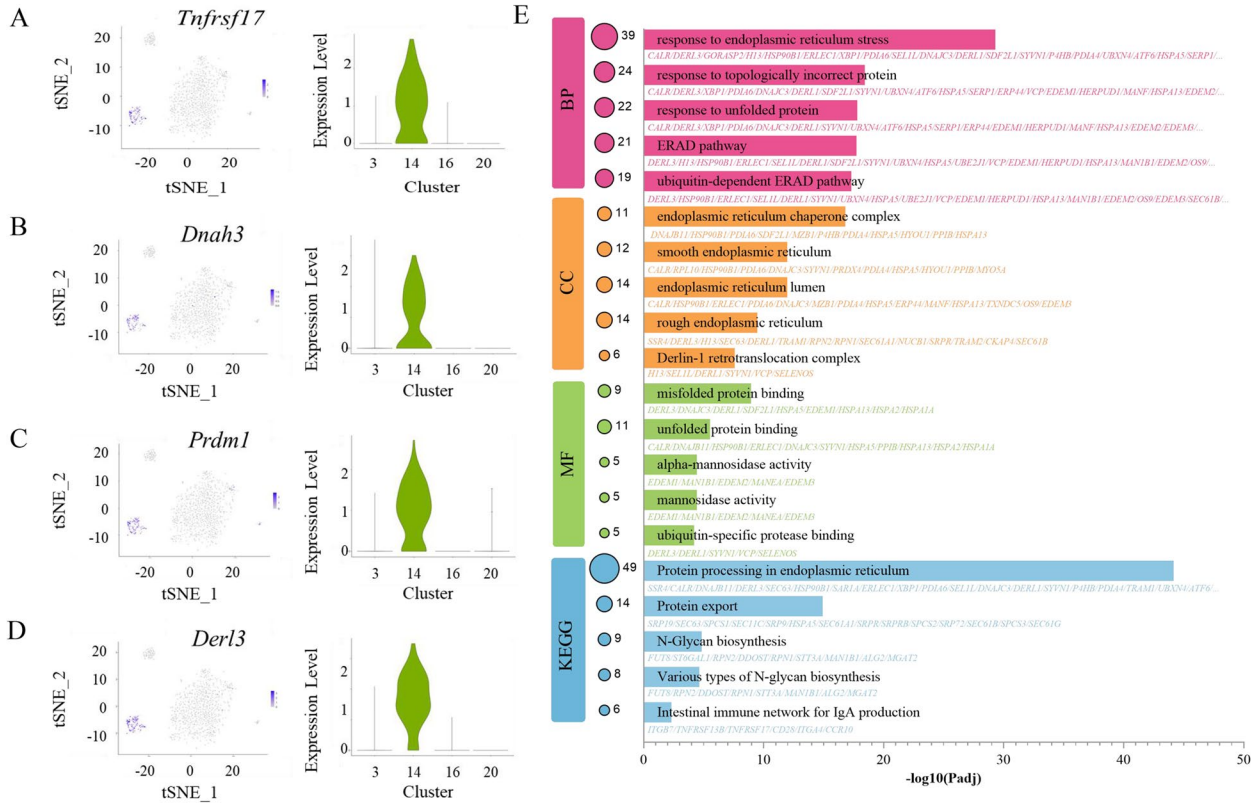

Fig. 3 Characteristics and biological functions of B cells in cluster 14. **A**-**D** Paired t-SNE plots (left) and violin plots (right) showed the expression levels of specific DEGs including *Tnfrsf17* (**A**), *Dnah3* (**B**), *Prdm1* (**C**) and *Derl3* (**D**) in cluster 14. **E** GO analysis and KEGG pathway enrichment of B cells distributed in cluster 14

GO enrichment analysis revealed BP related to interferon-γ response, cytokine-mediated signaling pathway, antigen processing and presentation, leukocyte cell–cell adhesion, and T cell activation; CC associated with lysosome, lytic vacuole, late endosome, MHC protein complex, and endosome membrane; and MF including enzyme activator activity, actin binding, cytokine receptor activity(Fig. 5D). KEGG pathway analysis further demonstrated enrichment in apoptosis, NF-κB, TNF, and JAK-STAT signaling pathways (Fig. 5D).

These findings identify a rare intrahepatic Apol7c$^+$ B cell subset that is diminished in MASH. Enrichment analyses indicate associations with apoptosis and inflammatory signaling pathways (NF-κB, TNF, and JAK-STAT), but the biological function of this subset in MASH remains to be experimentally validated.

The expressions of 4 sets of DEGs in each B cell cluster through hepatocytes-B cells coculture study

To further investigate the expressions of four sets of high specific DEGs in each cluster through hepatocytes-B cells coculture systems to understand whether lipotoxic hepatocytes mediating the inhibitory immune effect on B cells. GM12878 B cells were cultured in conditioned medium (CM) from HepG2 cells stimulated with 200μM PA (CM-PA) or BSA (CM-BSA). The mRNA of *Fcer2α*, *Cd22*, *Cr2* and *Fcmr* of cluster 3 were unifiedly downregulated in GM12878 cells incubated in the CM-PA versus CM-BSA ($p < 0.05$, Fig. 6A). In cluster 14, the mRNA of *Tnfrsf17*, *Prdm1* and *Derl3* were consistently downregulated in CM-PA group compared with CM-BSA, except for *Dnah3* ($p < 0.05$, Fig. 6B). Compared to CM-BSA, CM-PA exhibited a downregulated effect on *Chdh*, whereas an upregulated effect on *Dntt* and *Klk1* in cluster 16 ($p < 0.05$, Fig. 6C). In cluster 20, CM-PA coculture resulted in lower mRNA levels of *Apol1 (Apol7c)* and *Arhgap22* compared to CM-BSA, except for *Lad1* ($p < 0.05$, Fig. 6D). PA-HepG2–conditioned medium altered multiple cluster-associated B-cell transcripts, supporting hepatocyte-mediated regulation of B cells under lipotoxic stress; however, the causal relationship in vivo remains unclear. As cluster 3 represents the major hepatic B-cell subset and all four of its DEGs were consistently downregulated, we next focused on *Fcer2α* for further validation.

Presence of Fcer2α + B cells subpopulation in MASH mice livers

To determine the alteration of *Fcer2α*$^+$ B cells in MASH, we assessed the percentage of *Fcer2α*$^+$*Cd79a*$^+$ cells in liver

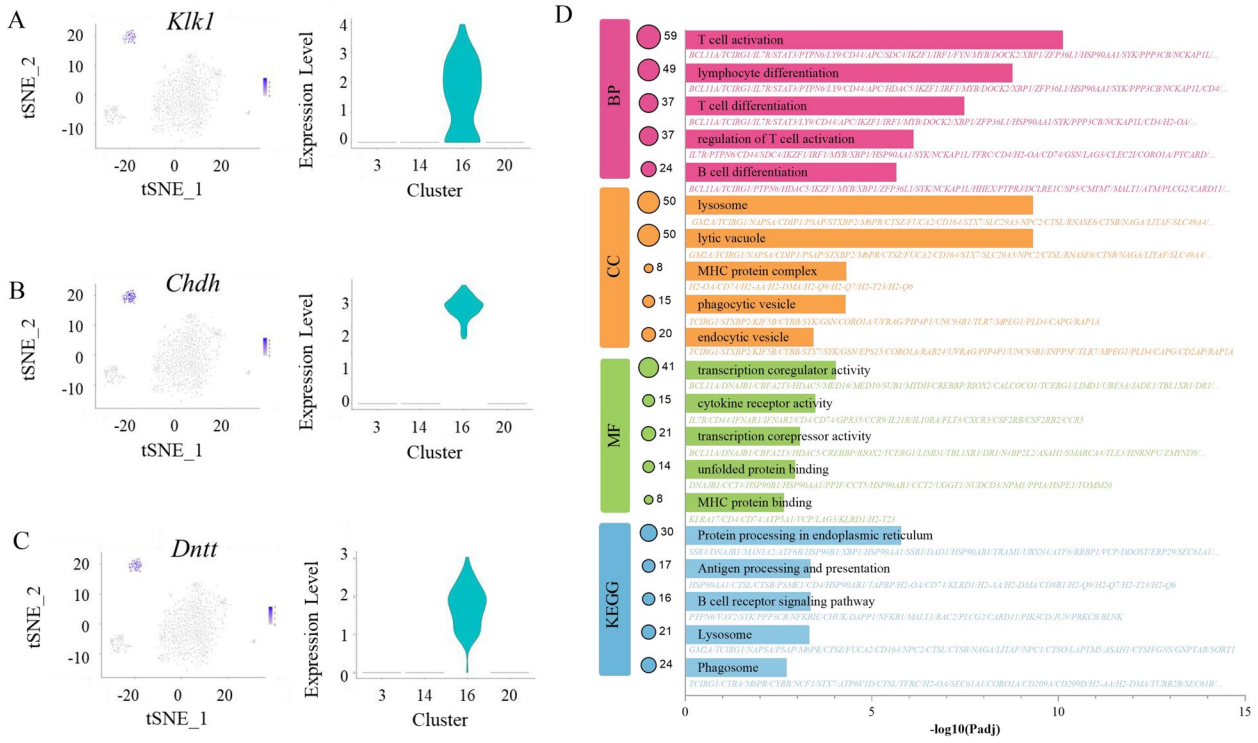

Fig. 4 Characteristics and biological functions of B cells in cluster 16. **A**-**C** Paired t-SNE plots (left) and violin plots (right) showed the expression levels of specific DEGs including *Klk1* (**A**), *Chdh* (**B**) and *Dntt* (**C**) in cluster 16. **D** GO analysis and KEGG pathway enrichment of B cells distributed in cluster 16

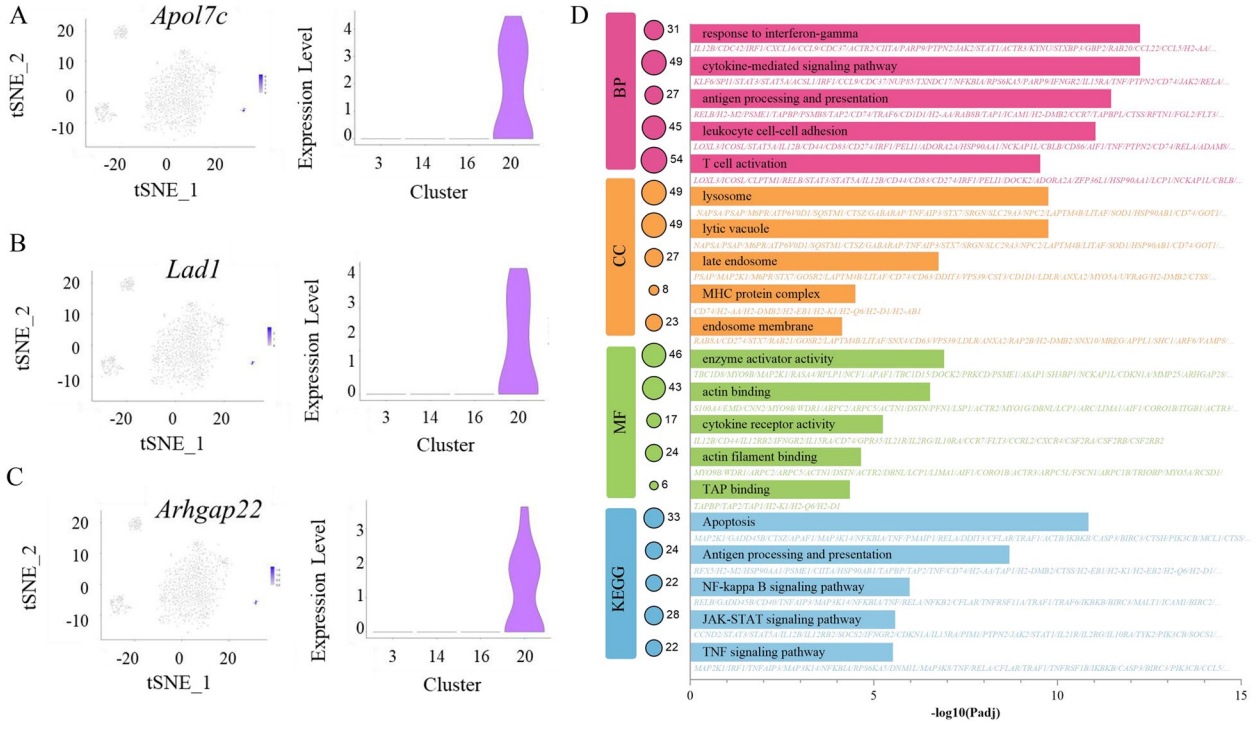

Fig. 5 Characteristics and biological functions of B cells in cluster 20. **A**-**C** Paired t-SNE plots (left) and violin plots (right) showing the expression levels of specific DEGs including *Apol7c* (**A**), *Lad1* (**B**) and *Arhgap22* (**C**) in cluster 20. **D** GO analysis and KEGG pathway enrichment of B cells distributed in cluster 20

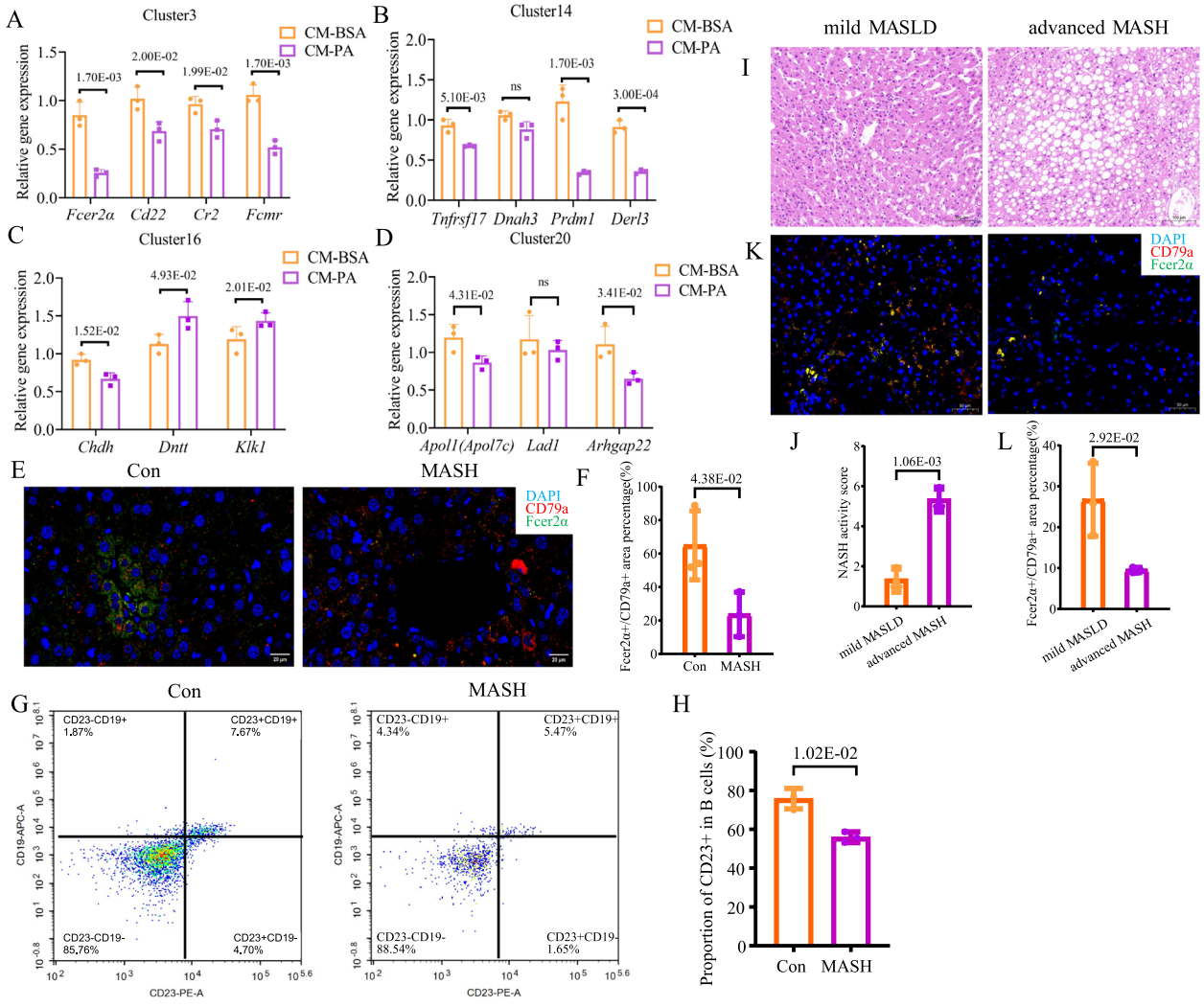

Fig. 6 Expression of cluster-specific DEGs and presence of *Fcer2a*⁺ B cells in MASH livers. The mRNA expressions of highly specific DEGs in each B cell cluster through hepatocytes-B cells coculture. GM12878 B cells cultured in CM-PA (from PA-treated HepG2) or CM-BSA (BSA-treated). The mRNA expressions of (**A**) *Fcer2a*, *Cd22*, *Cr2* and *Fcmr* of cluster 3; (**B**) *Tnfrsf17*, *Dnah3*, *Prdm1* and *Derl3* of cluster 14; (**C**) *Chdh*, *Dntt* and *Klk1* of cluster 16; (**D**) *Apol7c*, *Lad1* and *Arhgap22* of cluster 20 were examined by qRT-PCR. The presence of *Fcer2a*⁺ B cells in MASH livers was evaluated by IF staining. Two groups were established of MASH and control mice (each group, $n=3$). (**E**–**F**) Representative images and calculation of IF staining for Fcer2α (green IF) and Cd79a (red IF) in liver tissues (×400). Two groups were established of mild MASLD and advanced MASH patients (each group, $n=3$). (**G**-**H**) Representative flow cytometry plots and quantification of the proportion of *Fcer2a*⁺(CD23⁺) cells within the CD19⁺ B cell population(each group, $n=3$).Representative images and calculation of (**I**-**J**) H&E staining and (**K**-**L**) IF staining for Fcer2α (green IF) and Cd79a (red IF) of liver tissues from patient (×400). DAPI (blue) was used for nuclear staining. DAPI (blue) was used for nuclear staining

tissues of MASH mice by IF staining ($n=3$ per group). *Cd79a* served as a B cell marker. Nuclei were visualized by DAPI (blue IF). The portal area of liver tissues contained abundant *Fcer2α*⁺ (green IF) *Cd79a*⁺ (red IF) cells in control mice, but contained rare *Fcer2α*⁺*Cd79a*⁺ cells in MASH mice (MASH vs control group: 23.64 ± 10.88% vs 64.92 ± 6.87%, $p<0.05$, Fig. 6E-F).To independently validate this observation at the single-cell level, we performed flow cytometric analysis of liver-resident B cells. Consistent with the IF findings, the proportion of CD23⁺ (*Fcer2α*⁺) B cells was significantly lower in MASH mice than in controls (MASH vs control group: 55.93% ± 2.73% vs 75.79% ± 5.27%, $p<0.05$, Fig. 6G-H), corroborating a substantial reduction of the Fcer2*α*⁺ B-cell population in MASH.

Then we checked the percentage of *Fcer2α*⁺*Cd79a*⁺ cells in liver tissues of MASH patients by IF staining. Mild MASLD and advanced MASH was distinguished through H&E staining of liver tissues from patients (F ig. 6I-J). IF staining of human liver tissues showed a substantial decrease in *Fcer2α*⁺*Cd79a*⁺ cells in advanced MASH patients compared to mild MASLD controls (advanced MASH vs mild MASLD group: 9.50 ± 0.63% vs 26.70 ± 8.93%, $p<0.05$, Fig. 6K-L). These findings,

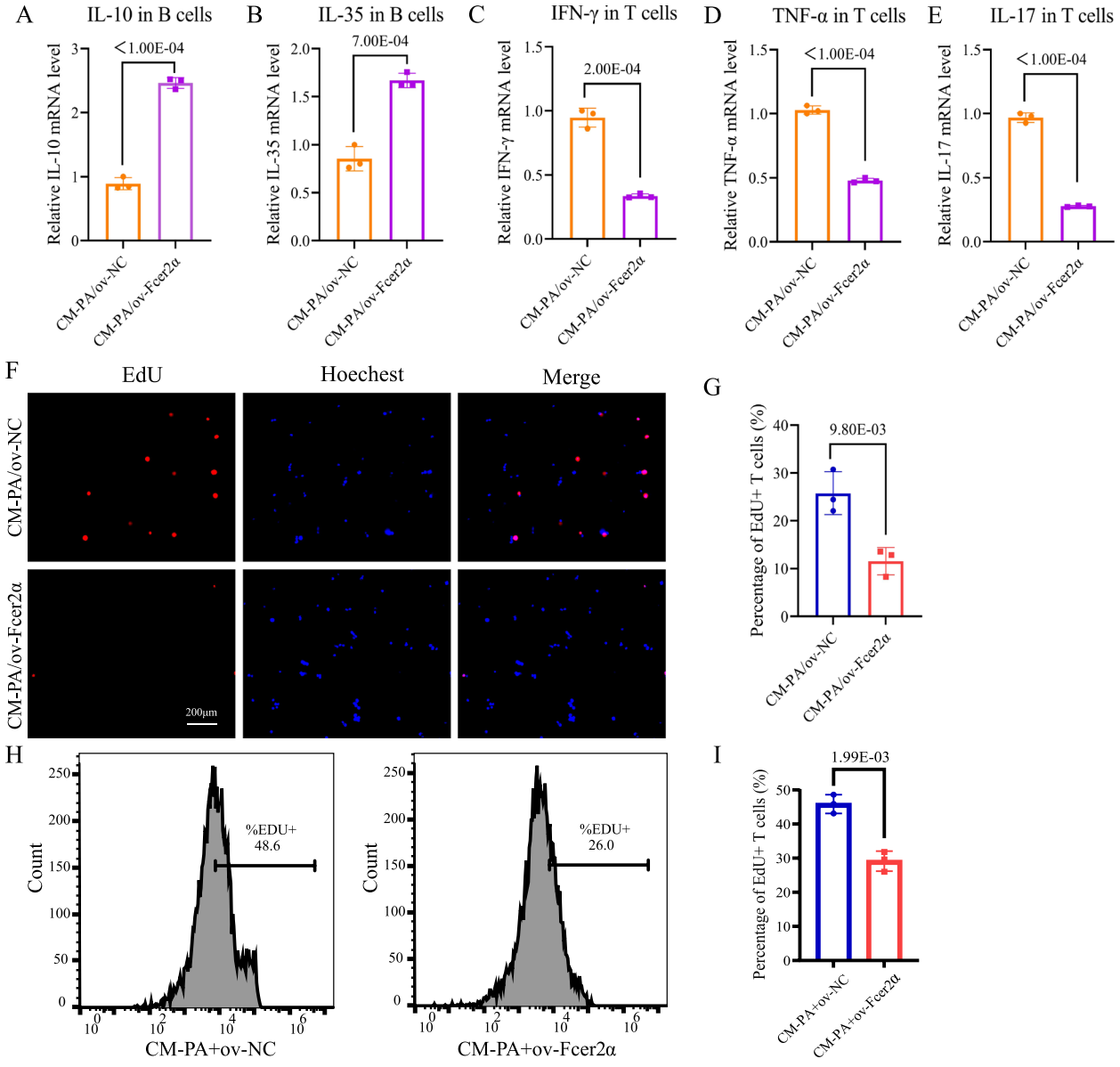

Fig. 7 Fcer2α.$^{+}$ B cells attenuated inflammation in the lipotoxic environment. **A**-**B** The mRNA expression of IL-10 and IL-35 in ov-*Fcer2α* B cells (ov-*Fcer2α*) versus control (ov-NC) cultured in CM-PA from PA-treated HepG2 cells (each group, $n=3$). **C**-**E** The mRNA levels of pro-inflammatory cytokines (IFN-γ, TNF-α, IL-17) of T cells and **F**-**G** Representative IF EdU staining (×400) and semi-quantification of T cells coculturing with ov-*Fcer2α* and ov-NC B cell groups in CM-PA (each group, $n=3$). **H**-**I** Representative flow cytometry histograms of EdU incorporation in T cells after coculture with ov-NC or ov-*Fcer2α* B cells in CM-PA, and quantification of the percentage of EdU^{+}T cells(each group, $n=3$)

consistent with scRNA-seq results, suggested the diminished *Fcer2α*$^{+}$ B cell subgroup was involved in MASH pathogenesis.

Fcer2α + B cells could attenuate inflammation in MASH

We further aimed to clarify the function of *Fcer2α*$^{+}$ B cells in MASH. Given that *Fcer2α*$^{+}$ B cells constituted the predominant hepatic B cell subset yet were significantly reduced in the livers of MASH, we established *Fcer2α* overexpressing (ov-*Fcer2α*) and the control (ov-NC) GM12878 cells in a lipotoxic model (cocultured in CM-PA from HepG2 cells). In lipotxic environment, *Fcer2α*-overexpressing B cells exhibited enhanced anti-inflammatory capacity, secreting 2.76-fold more IL-10 and 1.96-fold more IL-35 versus ov-NC cells ($p<0.05$; Fig. 7A-B).

Then KEGG pathway analysis implicated the *Fcer2α* signaling of B cells mainly regulated T cell differentiation; we next cocultured T cells (Jurkat cells) with ov-*Fcer2α* or ov-NC B cells (GM12878 cells) in the lipotoxic CM-PA. While coculturing with ov-*Fcer2α* B cells in the lipotoxic CM-PA, suppressed T cell-driven inflammation

occurred, as reducing IFN-γ, TNF-α, and IL-17 secretion of T cells (ov-*Fcer2α* group vs. ov-NC group by IFN-γ: 61.07 ± 4.40%, TNF-α: 54.90 ± 2.12%, IL-17: 69.07 ± 2.20%; $p < 0.05$; Fig. 7C-E) and diminishing T cell proliferation (EdU^+ cells in ov-*Fcer2α* group vs. ov-NC group: 11.55 ± 2.86% vs. 25.76 ± 4.49%; $p < 0.05$; Fig. 7F-G). Importantly, unbiased flow cytometric analysis further corroborated the reduction in T cell proliferation, showing a lower percentage of EdU^+ T cells in the ov-*Fcer2α* group compared with the ov-NC group (45.87 ± 4.26% vs. 28.72 ± 3.92%; $p < 0.05$; F ig. 7H-I).Therefore,in this lipotoxic coculture system,*Fcer2α* overexpression in B cells is associated with increased anti-inflammatory cytokine expression and a concomitant attenuation of T cell proliferative and pro-inflammatory responses, supporting a potential immunomodulatory role of *Fcer2α*$^+$ B cells under lipotoxic stress.

Discussion

MASLD/MASH is increasingly recognized as a major contributor to end-stage liver disease and is tightly linked to cardiometabolic comorbidities [21]. Rather than reiterating epidemiologic background, here we focus on interpreting how our scRNA-seq findings refine the understanding of intrahepatic B-cell states in MASH.

B cells participate in MASLD/MASH through cytokine/antibody secretion and regulation of immune activation. Prior work in diet-induced MASH models reported intrahepatic B-cell accumulation with inflammatory cytokine expression and T-cell activation [22], and Barrow et al. demonstrated B2 cell accumulation with increased IL-6 and TNF-α that promotes inflammation and fibrogenesis [4]. Recent scRNA-seq studies further support B-cell heterogeneity in MASH, including specific B-cell clusters [4], a Cxcl12/Cxcr4-high subset with fibrogenic features [23], and an overall reduction of hepatic B cells in MCD-induced MASH [24]. In our study, 21 major clusters of single-NPC were identified between MCD-induced MASH and control livers, with four single-B cell clusters characterized. Consistent with Deczkowska et al. [24], we observed a significant reduction in total hepatic B-cell proportion in MASH, indicating model-dependent remodeling rather than uniform expansion of B cells across MASH settings.

Interestingly, cluster 3 constituted the major hepatic B-cell cluster and displayed transcriptional features consistent with a *Fcer2α* (Cd23)-enriched B-cell state, together with functional annotations related to B-cell activation/differentiation, lymphocyte differentiation, lymphocyte proliferation, and T cell activation. Notably, this cluster was dominated by *Fcer2α*$^+$ B cells, and its proportion was markedly decreased in MASH. Although *Fcer2α*/CD23 has been reported in regulatory B-cell contexts with anti-inflammatory effects, such properties are context-dependent and CD23 expression alone is insufficient to define a canonical Breg population [25, 26]. In our study, we observed *Fcer2α* mRNA downregulation in lipotoxic B cells and a reduced abundance of portal *Fcer2α*$^+$ B cells in MASH patients/mice compared with controls. Moreover, functional assays showed that enhancing *Fcer2α* signaling in B cells was associated with an anti-inflammatory shift (increased anti-inflammatory mediator expression) and suppressed T-cell proliferation, supporting a potential immunomodulatory role of this *Fcer2α*$^+$ B-cell subset in a lipotoxic environment. Consistently, Ge et al. reported that $CD20^+$*Fcer2α*$^+$$IL10^+$ Breg-like cells can exert immunosuppressive effects [27]. Together, these findings suggest that depletion of the *Fcer2α*$^+$ B-cell-enriched cluster may contribute to an inflammatory milieu in MASH; however, in vivo causal validation will be required to firmly establish this mechanism.In addition to Fcer2α, cluster 3 also exhibited enrichment of Cr2, Fcmr, and Cd22, all of which were consistently downregulated in lipotoxic B cells. Cr2 has been proposed to be selected during B-cell transition and maturation under BCR-related signaling [28]. Fcmr deficiency has been linked to impaired B-cell tolerance with increased autoantibody production [29], and Cd22 functions as an inhibitory receptor that helps restrain B-cell activation and is implicated in protection against autoimmunity and B-cell malignancies [30]. Therefore, the coordinated reduction of these inhibitory/immune-modulatory signals in cluster 3 may be relevant to MASH-associated immune dysregulation and warrants further mechanistic investigation.

Activated B cells can differentiate into antibody-producing PCs. Antibodies mediate their effector functions by binding to Fc receptors on target cells or activating the complement system [31]. In mice fed a MCD diet to induce MASH, hepatic B2 cells can develop into IgG-producing plasma cells, which generate IgG against oxidative stress-derived epitopes (OSEs) [9]. The production of anti-OSE IgG is positively correlated with the severity of liver injury and lobular inflammation [10]. The cellular function of cluster 14 maybe related to ER stress and N-glycan biosynthesis. Cluster 14 mainly contained with *Tnfrsf17*$^+$ B cells and the proportion of them was decreased in MASH. Based on these observations, we preliminarily infer that although this plasma cell subset is decreased in overall number, the residual cells may exist in a highly activated and antibody-producing state.Indeed, *Tnfrsf17*$^+$ B cells typically induce pro-inflammatory cytokines (e.g., IL-6, TNF-α) in autoimmune diseases, thereby activating chronic inflammatory responses. Levels et al. reported that *Tnfrsf17* was upregulated in synovial tissue B cells from rheumatoid arthritis patients, where they promoted synovitis progression via the production of pathogenic autoantibodies [32].

Similarly, Kim et al. found systemic lupus erythematosus patients exhibited increasing *Tnfrsf17* expression on B cells, and enabled *Tnfrsf17*$^+$ B cells to drive inflammatory progression by enhancing TLR9-triggered secretion of anti-dsDNA and ANA autoantibodies [33].The role of *Tnfrsf17*$^+$ PCs requires further investigation.

Cluster 16, also a minor B cell group, was identified. In the same way, the cell function is activate, differentiate and regulate T cells. In our study, *Klk1* mRNA was upregulated in lipotoxic B cells. Zhang et al. identified Klk1 inhibition in the inflamed prostates; exogenous Klk1 restored endothelial function and exerted anti-inflammatory, antifibrotic, and antioxidative stress effects in the rat chronic-inflamed prostate [34]. The mechanism of *Klk1*$^+$ B cells remains unclear in MASH. Finally, the very small cluster 20 was enriched, and the cell function was inferred in dysregulation of apoptosis, NF-κB, TNF and JAK-STAT. *Apol7c* mRNA was downregulated in lipotoxic B cells in our study. Uzureau et al. previously linked *Apol7* knockdown to increased dendritic cell survival and *Apol7c* interaction with Bcl-xL [16]. But *Apol7c*$^+$ B cells were undefined in MASH. Overall, the roles of *Klk1*$^+$ and *Apol7c*$^+$ B-cell subsets in MASH remain undefined and should be tested in targeted protein-level and functional studies.

Several limitations of this study warrant mention. First, the number of captured B cells (1,106 in controls and 581 in MASH) restricts the resolution for identifying rare subpopulations and limits the assessment of biological variability across animals. Second, although we inferred cluster identities and potential functions using transcriptional signatures and in vitro assays, these findings remain largely correlative; in this context, our HepG2–GM12878 conditioned-medium coculture is a reductionist system that captures only hepatocyte-derived soluble factors and cannot fully recapitulate complex intrahepatic crosstalk in vivo. Third, while the MCD diet model reproduces steatohepatitis and fibrosis, it does not fully recapitulate the systemic metabolic features central to human MASLD/MASH, limiting its ability to model the metabolic inflammation that drives human disease and potentially constraining clinical translatability. Fourth, the human validation cohort is small ($n = 6$), which limits its statistical power and the generalizability of the human IF observations. Future studies should expand cohort sizes, incorporate more physiologically relevant models (high-fat diet and Western diet) alongside human samples, and perform targeted in vivo perturbation experiments to better reflect human pathology and rigorously validate the translational relevance of the proposed B-cell functions.

In summary, the composition of four undefined single-B cell subsets is altered in MASH. We identified a predominant *Fcer2α*$^+$ B-cell subset that is significantly reduced in MASH and may be linked to impaired immunomodulatory tone under lipotoxic stress, whereas the roles of the rarer subsets (clusters 14, 16, and 20) remain to be established.

Supplementary Information

The online version contains supplementary material available at https://doi.org/10.1186/s12876-026-04704-w.

Additional file 1: Table S1 Clinical, biochemical and histologic features of human. Table S2 Primers used in qRT-PCR. Table S3 Antibodies used in IF. Table S4. Top 10 DEGs of B cells of cluster 3. Table S5 Top 10 DEGs of B cells of cluster 14. Table S6 Top 10 DEGs of B cells of cluster 16. Table S7 Top 10 DEGs of B cells of cluster 20.

Authors' contributions

Conceived the study design: S.Z.L., M.L.X. and M.Y.X. Performed the experiments and analysed the data: T.M., Z.Q.C., H.Y.L. and J.C.L. Analysed the scRNA-seq data set: H.Y.L., L.T. and S.Z.L. Wrote the manuscript: M.Y.X.,J.C.L. and T.M.

Funding

This study was supported by the National Natural Science Foundation of China (No. 82270604).

Data availability

The datasets generated during the current study are available from the corresponding author on reasonable request.The single-cell RNA sequencing datasets generated and analyzed during the current study are available in the Gene Expression Omnibus (GEO) repository under accession number GSE225786.

Declarations

Ethics approval and consent to participate

All procedures performed in studies involving human participants were in accordance with the ethical standards of the institution and with the 1964 Helsinki Declaration. Written informed consent was obtained from individual or guardian participants. The study was approved by the Bioethics Committee of Shanghai East Hospital.The animal study was approved by the Institutional Animal Care and Use Committee of Shanghai East Hospital.

Consent for publication

Not Applicable.

Competing interests

The authors declare no competing interests.

Received: 28 October 2025 / Accepted: 19 February 2026
Published online: 25 February 2026

References

1. Allen AM, Lazarus JV, Younossi ZM. Healthcare and socioeconomic costs of NAFLD: a global framework to navigate the uncertainties. J Hepatol. 2023;79(1):209–17.
2. Rui L, Lin JD. Reprogramming of hepatic metabolism and microenvironment in nonalcoholic steatohepatitis. Annu Rev Nutr. 2022;42:91–113.
3. Barrow F, Khan S, Wang H, et al. The emerging role of B cells in the pathogenesis of NAFLD. Hepatology. 2021;74(4):2277–86.
4. Barrow F, Khan S, Fredrickson G, et al. Microbiota-driven activation of intrahepatic B cells aggravates NASH through innate and adaptive signaling. Hepatology. 2021;74(2):704–22.
5. Kotsiliti E, Leone V, Schuehle S, et al. Intestinal B cells license metabolic T-cell activation in NASH microbiota/antigen-independently and contribute to fibrosis by IgA-FcR signalling. J Hepatol. 2023;79(2):296–313.

6. Younossi ZM, Loomba R, Anstee QM, et al. Diagnostic modalities for nonalcoholic fatty liver disease, nonalcoholic steatohepatitis, and associated fibrosis. Hepatology. 2018;68:349–60.
7. Li HY, Fu SW, Wu JC, et al. Vsig4+ resident single-Kupffer cells improve hepatic inflammation and fibrosis in NASH. Inflamm Res. 2023;72(4):669–82.
8. Rafiei H, Yeung M, Kowalski S, et al. Development of a novel human triculture model of non-alcoholic fatty liver disease and identification of berberine as ameliorating steatosis, oxidative stress and fibrosis. Front Pharmacol. 2023;19(14):1234300.
9. Bruzzì S, Sutti S, Giudici G, et al. B2-lymphocyte responses to oxidative stress-derived antigens contribute to the evolution of nonalcoholic fatty liver disease (NAFLD). Free Radic Biol Med. 2018;124:249–59.
10. Sutti S, Jindal A, Locatelli I, et al. Adaptive immune responses triggered by oxidative stress contribute to hepatic inflammation in NASH. Hepatology. 2014;59(3):886–97.
11. Mabbott NA, Gray D. Identification of co-expressed gene signatures in mouse B1, marginal zone and B2 B-cell populations. Immunology. 2014;141(1):79–95.
12. Takahashi K, Kozono Y, Waldschmidt TJ, et al. Mouse complement receptors type 1 (CR1;CD35) and type 2 (CR2;CD21): expression on normal B cell subpopulations and decreased levels during the development of autoimmunity in MRL/lpr mice. J Immunol. 1997;159(3):1557–69.
13. Zhang YR, Yu Z, Xiong WJ, et al. TOSO interacts with SYK and enhances BCR pathway activation in chronic lymphocytic leukemia. Chin Med J (Engl). 2020;133(17):2090–7.
14. Duan S, Paulson JC. Siglecs as immune cell checkpoints in disease. Annu Rev Immunol. 2020;38:365–95.
15. Eslami M, Schneider P. Function, occurrence and inhibition of different forms of BAFF. Curr Opin Immunol. 2021;71:75–80.
16. Sabat R, Šimaitė D, Gudjonsson JE, et al. Neutrophilic granulocyte-derived B-cell activating factor supports B cells in skin lesions in hidradenitis suppurativa. J Allergy Clin Immunol. 2023;151(4):1015–26.
17. Klein U, Casola S, Cattoretti G, et al. Transcription factor IRF4 controls plasma cell differentiation and class-switch recombination. Nat Immunol. 2006;7(7):773–82.
18. Lin L, Lin G, Lin H, et al. Integrated profiling of endoplasmic reticulum stress-related DERL3 in the prognostic and immune features of lung adenocarcinoma. Front Immunol. 2022;13:906420.
19. Leu CH, Yang ML, Chung NH, et al. Kallistatin ameliorates influenza virus pathogenesis by inhibition of kallikrein-related peptidase 1-mediated cleavage of viral hemagglutinin. Antimicrob Agents Chemother. 2015;59(9):5619–30.
20. Uzureau S, Coquerelle C, Vermeiren C, et al. Apolipoproteins L control cell death triggered by TLR3/TRIF signaling in dendritic cells. Eur J Immunol. 2016;46(8):1854–66.
21. Byrne CD, Targher G. Nafld: a multisystem disease. J Hepatol. 2015;62(1 Suppl):S47–64.
22. Zhang F, Jiang WW, Li X, et al. Role of intrahepatic B cells in non-alcoholic fatty liver disease by secreting pro-inflammatory cytokines and regulating intrahepatic T cells. J Dig Dis. 2016;17(7):464–74.
23. Xiong X, Kuang H, Ansari S, et al. Landscape of intercellular crosstalk in healthy and NASH liver revealed by single-cell secretome gene analysis. Mol Cell. 2019;75:644–60.
24. Deczkowska A, David E, Ramadori P, et al. XCR1(+) type 1 conventional dendritic cells drive liver pathology in non-alcoholic steatohepatitis. Nat Med. 2021;27(6):1043–54.
25. Rosser EC, Mauri C. Regulatory B cells: origin, phenotype, and function. Immunity. 2015;42(4):607–12.
26. Rafei M, Hsieh J, Zehntner S, et al. A granulocyte-macrophage colony-stimulating factor and interleukin-15 fusokine induces a regulatory B cell population with immune suppressive properties. Nat Med. 2009;15(9):1038–45.
27. Ge Q, Zhou S, Lu J, et al. Regulatory B cells promote the immunosuppressive microenvironment and progression of clear cell renal cell carcinoma. Immunother Adv. 2025;5(1):ltaf013.
28. Allman D, Pillai S. Peripheral B cell subsets. Curr Opin Immunol. 2008;2008(20):149–57.
29. Kubagawa H, Mahmoudi Aliabadi P, Al-Qaisi K, et al. Functions of IgM fc receptor (FcR) related to autoimmunity. Autoimmunity. 2024;57(1):2323563.
30. Röder B, Nitschke L. The role of Siglec-G on B cells in autoimmune disease and leukemia. Semin Arthritis Rheum. 2024;64S:152328.
31. Akkaya M, Kwak K, Pierce SK. B cell memory: building two walls of protection against pathogens. Nat Rev Immunol. 2020;20(4):229–38.
32. Levels MJ, Van Tok MN, Cantaert T, et al. The transcriptional coactivator Bob1 is associated with pathologic B cell responses in autoimmune tissue inflammation. Arthritis Rheumatol. 2017;69(4):750–62.
33. Kim J, Gross JA, Dillon SR, et al. Increased BCMA expression in lupus marks activated B cells, and BCMA receptor engagement enhances the response to TLR9 stimulation. Autoimmunity. 2011;44(2):69–81.
34. Zhang M, Lin D, Luo C, et al. Tissue kallikrein protects rat prostate against the inflammatory damage in a chronic autoimmune prostatitis model via restoring endothelial function in a bradykinin receptor B2-dependent way. Oxid Med Cell Longev. 2022;2022:1247806.

Publisher's Note